Brownian Dynamics of Confined Suspensions of Active Microrollers

Florencio Balboa Usabiaga, Blaise Delmotte, and Aleksandar Donev

Courant Institute of Mathematical Sciences,

New York University, New York, NY 10012, USA

We develop efficient numerical methods for performing many-body Brownian dynamics simulations of a recently-observed fingering instability in an active suspension of colloidal rollers sedimented above a wall [M. Driscoll, B. Delmotte, M. Youssef, S. Sacanna, A. Donev and P. Chaikin, Nature Physics, 2016, doi:10.1038/nphys3970]. We present a stochastic Adams-Bashforth integrator for the equations of Brownian dynamics, which has the same cost as but is more accurate than the widely-used Euler-Maruyama scheme, and uses a random finite difference to capture the stochastic drift proportional to the divergence of the configuration-dependent mobility matrix. We generate the Brownian increments using a Krylov method, and show that for particles confined to remain in the vicinity of a no-slip wall by gravity or active flows the number of iterations is independent of the number of particles. Our numerical experiments with active rollers show that the thermal fluctuations set the characteristic height of the colloids above the wall, both in the initial condition and the subsequent evolution dominated by active flows. The characteristic height in turn controls the timescale and wavelength for the development of the fingering instability.

I. INTRODUCTION

Colloidal particles suspended in a liquid often sediment towards a bottom wall due to gravity, or are confined to move between two parallel walls. For example, quasi-two-dimensional experiments use optical microscopy [1, 2] or light scattering techniques [3] to observe colloidal particles confined between microscopes slips. Synthetic active colloids are usually metallic [4, 5] or have metallic components [6, 7], making them much denser than the surrounding fluid and therefore prone to sediment towards the floor. Even neutrally buoyant active colloids are often advected toward the boundaries by the active flows [8]. If the walls are well separated and the colloids remain much closer to one of the walls, one can model the system as a colloidal suspension in a half-space bounded by an infinite no-slip wall [9]. This framework is useful to study both passive [10] and active suspensions [8, 11].

Despite the large number of experiments dealing with colloidal suspensions close to a single wall, there are few computational many-body simulations in this geometry. For active suspensions, Spagnolie et al. [12] and Lushi et al [13] both developed minimal models of swimmer cells (an axisymmetric swimmer and a bi-flagellated algae respectively) with consistent hydrodynamic interactions with a nearby wall. However, they did not include thermal fluctuations nor considered many-body hydrodynamic interactions. In a previous work we consider many body simulations of arbitrary shaped passive or active colloids near a planar wall using a rigid multiblob method [14], however, we did not discuss how to include Brownian motion. Recently, Singh and Adhikari [11] have used a Galerkin boundary integral representation for active spheres [15] to study the crystallization of a two-dimensional rotating suspension of spheres near a boundary; similar crystal behavior has been observed in experiments with bacteria and synthetic active colloids [6, 16], as well in simulations of unconfined rotating spheres [17, 18]. These studies neglect all Brownian motion because their magnitude is estimated to be small compared with the active forces. Other works that focus on active suspensions have been published but in general they do not include Brownian fluctuations or many-body hydrodynamic interactions [19–21].

For passive suspensions, Michailidou et al. [10] and Lele et al. [22] combined experiments with Stokesian Dynamics (SD) simulations [23] to study colloidal suspensions close to a wall. Michailidou et al. [10] studied the diffusive behavior of concentrated colloidal suspension through light scattering methods; however, they only used SD simulations to solve the

mobility problem in a two particle system and they did not consider Brownian motion. Lele et al. [22] investigated the diffusive modes of a small colloidal cluster (formed by seven particles) using optical microscopy. Their SD simulations included hydrodynamic interactions [9, 23] and Brownian motion [24] but only for their seven-particle cluster.

It is difficult to perform large-scale Brownian Dynamics (BD) with hydrodynamic interactions for particles confined near an infinite planar no-slip boundary using existing numerical methods. The first key difficulty is efficiently generating the particles' Brownian displacement. Specifically, it is necessary to generate random displacements with a covariance proportional to the hydrodynamic *mobility matrix* as to obey fluctuation-dissipation balance. Fixman proposed an iterative method to generate this Brownian noise. His key idea was to realize that it is enough to obtain an approximation to the noise with a tolerance much looser than the machine precision. He proposed to use Chebyshev polynomials to approximate the Brownian noise [25]. Fixman's method has become extremely popular in the chemical engineering community despite its known shortcommings. Importantly, Fixman's method requires knowing the largest and smallest eigenvalues of the mobility matrix, which requires to use another iterative method [26]. Moreover, Fixman's method often does not converge uniformly and the number of iterations to achieve a given tolerance generally increases with the number of particles [27]. For periodic or confined domains one can use a fluid solver to compute the action of the mobility on the fly [28–30]. One can combine this technique with the Fixman's iterative method [31] to generate the Brownian displacements. However, this approach requires a Stokes solve every iteration and it is therefore expensive. One can instead use fluctuating hydrodynamics [30, 32, 33]. In this approach one first generates a random velocity consistent with the fluctuating steady Stokes equations on a grid, and then one interpolates this random velocity to the particle positions [30, 32]. However, fluctuating hydrodynamics is not straightforward in the geometry of interest here since it is not possible to use an infinite grid to cover the half-space above the wall.

To reproduce the equilibrium Gibbs-Boltzmann distribution it is necessary to introduce in the BD equations a well-known stochastic drift term proportional to the divergence of the mobility matrix [30, 32]. Doing this efficiently and accurately is a second key difficulty in performing Brownian dynamics, especially in non-periodic domains [30]. Again, Fixman proposed a method to compute this contribution. His idea was to use a midpoint temporal integrator to approximately include the drift term [34]. However, the midpoint scheme of

Fixman not only involves the square root of the mobility but also the square root of its inverse, the resistance matrix. Since there is no pairwise approximations to the resistance matrix even considering only far field hydrodynamic interactions [35], solving resistance problems is generally notably harder than solving mobility problems [14, 36]. This makes Fixman's midpoint scheme expensive in practice [37], especially in unbounded systems where the mobility matrix is ill-conditioned.

Here we combine two techniques developed in recent years to overcome the challenges of performing many-body Brownian simulations for particles confined above a no-slip boundary. We include the effect of the thermal drift using *random finite differences* (RFD) [30, 38]. To generate random displacements with the correct covariance, we use an efficient iterative method based on Krylov polynomial approximations [27, 39, 40]. We find that the screening of hydrodynamics by the nearby boundary makes the hydrodynamic interactions sufficiently short-ranged to make the number of iterations required to achieve a given tolerance *independent* of the number of particles, making our method scalable to hundreds of thousands of particles. In this work we only include hydrodynamic interactions in a far field approximation and do not use a preconditioner [40]. However, it is important to note that both the RFD and the Krylov method are general techniques that can effectively be used with other methods such as the boundary integral method of Adhikari et al. [11, 15] or our rigid multiblob method [14], with an appropriate preconditioner.

In a recent publication some of us performed simulations with thousands of colloidal particles to study a fingering hydrodynamic instability in a suspension of active rollers [7]. In a series of experiments, magnetic colloids roll above a floor with a specific angular frequency set by an external magnetic field. The flow created by the rotation of the colloids creates a strong collective motion. After the formation of a shock front of finite width, a fingering instability appears in the direction transverse to the particles' motion with the fingers traveling faster than the rest of the suspension. In the simulations we observed that these fingers can detach from the suspension and form persistent motile structures of a well defined size, termed "critters", which move above the wall at high speed compared with a single particle. Quite remarkably, the shock, fingers and clusters are formed solely due to hydrodynamic interactions in the presence of the bottom wall. In our previous work we did not include the effect of Brownian motion. While the Péclet number in this active suspension is large, $\mathrm{Pe} \sim 30$, the effect of thermal noise is key since it sets the characteristic

height of the colloids above the no-slip wall. Moreover, Brownian motion will tend to break the stable hydrodynamic clusters observed in the absence of fluctuations. In this paper we continue the study of this active suspension by including the effect of thermal fluctuations in simulations with approximately thirty thousand particles.

In Sec. II we present the equations of Brownian dynamics and the tools to solve them efficiently. Then, in Sec. III we study the effects of Brownian motion in an active suspension of Brownian rollers. We conclude the paper with a summary and discussion in Sec. IV. Some technical results are discussed in the Appendices.

II. BROWNIAN DYNAMICS OF CONFINED SUSPENSIONS

The Brownian dynamics of N colloidal particles with coordinates $\boldsymbol{q}(t) = \{\boldsymbol{q}_1(t), \ldots, \boldsymbol{q}_N(t)\}$ immersed in a viscous fluid can be described with the Ito stochastic equation

$$\frac{\mathrm{d}\boldsymbol{q}}{\mathrm{d}t} = \boldsymbol{M}\boldsymbol{F} + \sqrt{2k_BT}\boldsymbol{M}^{1/2}\boldsymbol{\mathcal{W}} + (k_BT)\,\partial_q \cdot \boldsymbol{M}, \tag{1}$$

where $\boldsymbol{M}(\boldsymbol{q})$ is the mobility matrix that couples particles (translational) velocities to applied forces $\boldsymbol{F}(\boldsymbol{q};t)$, k_B and T are the Boltzmann constant and the temperature, and $\boldsymbol{\mathcal{W}}(t)$ is a vector of independent white noise processes with zero mean and covariance $\langle \boldsymbol{\mathcal{W}}(t)\boldsymbol{\mathcal{W}}^T(t')\rangle = \boldsymbol{I}\delta(t-t')$. The "square root" of the mobility matrix is any matrix (not necessarily square) that ensures that the Gaussian noise has a covariance proportional to the mobility matrix, i.e., that the *fluctuation-dissipation balance* condition

$$\boldsymbol{M}^{1/2}\left(\boldsymbol{M}^{1/2}\right)^T = \boldsymbol{M}, \tag{2}$$

holds for all $\boldsymbol{q}$. Equation (1) has been used frequently to simulate colloids [23] and polymers [26], however, it presents some challenges if one wants to solve it efficiently for thousands of particles interacting hydrodynamically with a nearby wall.

A. Temporal integrators

Second order weakly accurate temporal integrators have been proposed for stochastic equations with multiplicative noise, see for example Refs. [41, 42]. However, these schemes are too expensive to solve (1) for tens to hundreds of thousands of particles. Therefore,

we focus here on weakly first order accurate methods, the simplest of which is the Euler-Maruyama (EM) scheme,

$$\begin{aligned}\boldsymbol{q}^{n+1} = \boldsymbol{q}^n + \Delta t \boldsymbol{M}^n \boldsymbol{F}^n + \sqrt{2k_BT\Delta t}\,(\boldsymbol{M}^n)^{1/2}\,\boldsymbol{W}^n \\ +\Delta t \frac{k_BT}{\delta}\left[\boldsymbol{M}\left(\boldsymbol{q}^n + \frac{\delta}{2}\widetilde{\boldsymbol{W}}^n\right)\widetilde{\boldsymbol{W}}^n - \boldsymbol{M}\left(\boldsymbol{q}^n - \frac{\delta}{2}\widetilde{\boldsymbol{W}}^n\right)\widetilde{\boldsymbol{W}}^n\right],\end{aligned} \tag{3}$$

where Δt is the time step size, superscripts indicates the point at which quantities are evaluated (e.g., $\boldsymbol{q}^n = \boldsymbol{q}(t = n\Delta t)$ and $\boldsymbol{M}^n = \boldsymbol{M}(\boldsymbol{q}^n)$), δ is a small length compared with the particle radius a, and $\boldsymbol{W}^n$ and $\widetilde{\boldsymbol{W}}^n$ are uncorrelated vectors of independent identically distributed (i.i.d.) standard normal variates.

The last term in Eq. (3) is a centered *random finite difference* (RFD) approximation to the stochastic drift term that is equal in expectation to $\Delta t k_BT\,(\partial_q \cdot \boldsymbol{M})^n$ for sufficiently small δ; one can also use a one-sided difference. The RFD term guarantees that the EM scheme is a consistent integrator of (1) [30, 38], but is simpler and more efficient in practice than the Fixman midpoint scheme. Assuming that the product between the mobility matrix $\boldsymbol{M}$ and a force vector is computed with accuracy ε, and denoting the radius of the particles with a, a balance between truncation and roundoff error in the centered RFD is achieved for $\delta/a \sim \varepsilon^{1/3}$ ($\delta/a \sim \varepsilon^{1/2}$ for one-sided difference); choosing $\delta/a = 10^{-6} - 10^{-5}$ is appropriate for the simulations reported here.

The EM scheme (3) is not particularly accurate even for deterministic equations. Another first order weakly accurate scheme that we empirically find to give notably better accuracy is the stochastic Adams-Bashforth (AB) scheme,

$$\begin{aligned}\boldsymbol{q}^{n+1} = \boldsymbol{q}^n + \Delta t\left[\frac{3}{2}\boldsymbol{M}^n\boldsymbol{F}^n - \frac{1}{2}\boldsymbol{M}^{n-1}\boldsymbol{F}^{n-1}\right] + \sqrt{2k_BT\Delta t}\,(\boldsymbol{M}^n)^{1/2}\,\boldsymbol{W}^n \\ +\Delta t \frac{k_BT}{\delta}\left[\boldsymbol{M}\left(\boldsymbol{q}^n + \frac{\delta}{2}\widetilde{\boldsymbol{W}}^n\right)\widetilde{\boldsymbol{W}}^n - \boldsymbol{M}\left(\boldsymbol{q}^n - \frac{\delta}{2}\widetilde{\boldsymbol{W}}^n\right)\widetilde{\boldsymbol{W}}^n\right].\end{aligned} \tag{4}$$

Here we use the same Brownian displacement as in (3) but we evaluate the deterministic forces with a second order method. Observe that the AB and EM schemes have the same computational cost per time step, with the only difference being that the AB scheme requires storing one more vector. We are not aware of an analysis of the weak accuracy of multistep schemes such as (4), however, we demonstrate empirically in Appendix B that the AB scheme improves not only the deterministic but also the stochastic accuracy for time step sizes that resolve all relevant physical time scales. One could build other integrators based on the mid-point or the trapezoidal rules [43] at the cost of increasing the cost per time step.

We have found that the AB scheme has a similar tradeoff of accuracy versus computational cost as two steps Runge-Kutta methods. We we use the AB scheme here because it is more efficient in the deterministic setting.

B. Mobility matrix

To make (1) well-posed, we need a mobility matrix $\boldsymbol{M}$ that is symmetric positive semidefinite (SPD) for all particle configurations. In the presence of an infinite no-slip wall the mobility should include the effect of the wall on the hydrodynamic interactions. We use a standard pairwise approximation that includes the long-range contribution. For spherical particles of radius a we can write the pair mobility matrix between two different particles i and j using the generalized Rotne-Prager (RP) tensor $\boldsymbol{\mathcal{R}}$ [9, 44],

$$\boldsymbol{M}_{ij} = \boldsymbol{\mathcal{R}}\left(\boldsymbol{q}_i, \boldsymbol{q}_j\right) = \left(\boldsymbol{I} + \frac{a^2}{6}\boldsymbol{\nabla}_x^2\right)\left(\boldsymbol{I} + \frac{a^2}{6}\boldsymbol{\nabla}_y^2\right)\boldsymbol{G}(\boldsymbol{x}, \boldsymbol{y})\Big|_{\boldsymbol{x}=\boldsymbol{q}_i}^{\boldsymbol{y}=\boldsymbol{q}_j}, \tag{5}$$

where $\boldsymbol{G}(\boldsymbol{x}, \boldsymbol{y})$ is the Green's function of the Stokes equation with the appropriate boundary conditions, and the parentheses are the Faxén operators. Blake found the Green's function for the Stokes problem in a half space using a method of images [45], and Swan and Brady have used this to compute explicit expressions for the RP tensor (5) in the presence of a wall [9].

A practical problem of the mobility given by Swan and Brady [9] is that it only remains positive semidefinite if the particles do not overlap with each other or with the wall. The no-overlap requirement seems natural; however, to completely avoid overlaps in a BD simulation it is necessary to use very strong repulsive potentials and therefore small time step sizes. We prefer to use softer potentials that allow for larger time step sizes at the cost of an occasional overlap; therefore, we need to generalize the mobility matrix to have a positive semidefinite expression for all particle configurations.

For particles overlapping with each other, instead of applying the Faxén operators to the Green's function as in Eq. (5) one can compute the mobility in two steps. The first step is to compute the flow $\boldsymbol{v}(\boldsymbol{r})$ created by a force density $\boldsymbol{F}/(4\pi a^2)$ acting on the surface S_i of one of the spheres. The second step is to compute the velocity of the second particle as the average of the velocity flow $\boldsymbol{v}(\boldsymbol{r})$ over the surface S_j of the other particle. This leads to the

integral form of the Rotne-Prager-Yamakawa (RPY) tensor [44],

$$\boldsymbol{\mathcal{R}}\left(\boldsymbol{q}_i, \boldsymbol{q}_j\right) = \frac{1}{(4\pi a^2)^2} \oint_{\boldsymbol{x}\in S_i} \oint_{\boldsymbol{y}\in S_j} \boldsymbol{G}(\boldsymbol{x}, \boldsymbol{y})\, dS_i(\boldsymbol{x}) dS_j(\boldsymbol{y}), \tag{6}$$

which is identical to the differential form (5) for non-overlapping particles. For particles that overlap each other but do not overlap the wall, it has been shown that the correction relative to (5) is independent of the boundary conditions [44], and therefore it is the same as the one obtained by Rotne and Prager in an unbounded domain [46]. Specifically, the RPY mobility (6) in the presence of a wall that we use in this work is given by adding the wall-corrections given in Eqs. (B1) and (C2) in [9] to the RPY tensor in an unbounded domain given in Eq. (3.12) in [44]. Note that the self-mobility of a particle is given by (6) with $j = i$. Equation (6) cannot be applied directly when one or both of the particles overlap the wall because part of the particles surface extends beyond the wall. In Appendix A we explain how we regularize the mobility matrix for particles overlapping the wall so that $\boldsymbol{M}$ is SPD for all particle configurations.

We use a simple direct summation implemented in PyCUDA [47], which runs in Graphical Processing Units (GPUs), to compute the matrix vector product $\boldsymbol{MF}$. Although the computational cost of this method is formally $\mathcal{O}(N^2)$ in the number of particles N, the GPUs allow for a high parallelization of the calculation making this part of the algorithm fast enough to be used with thousands of particles [48]. We want to point out that in certain circumstances the matrix vector product can be computed in a quasi-linear time in the number of particles. For example, for periodic domains one can compute the matrix vector product using Ewald splitting methods [33], and for unbounded domains one can use Fast Multipole Methods (FMM) [39]. For the half-space problem it is also known how to use FMM in the limit $a \to 0$ (i.e. for Stokeslets) [49], but not for $a > 0$, to our knowledge. When deciding which method should be used one has to bear in mind that often, a simple GPU implementation can be faster than a method with a better theoretical scaling unless the number of particles is above about a hundred thousand for present-day hardware and FMM implementations [14].

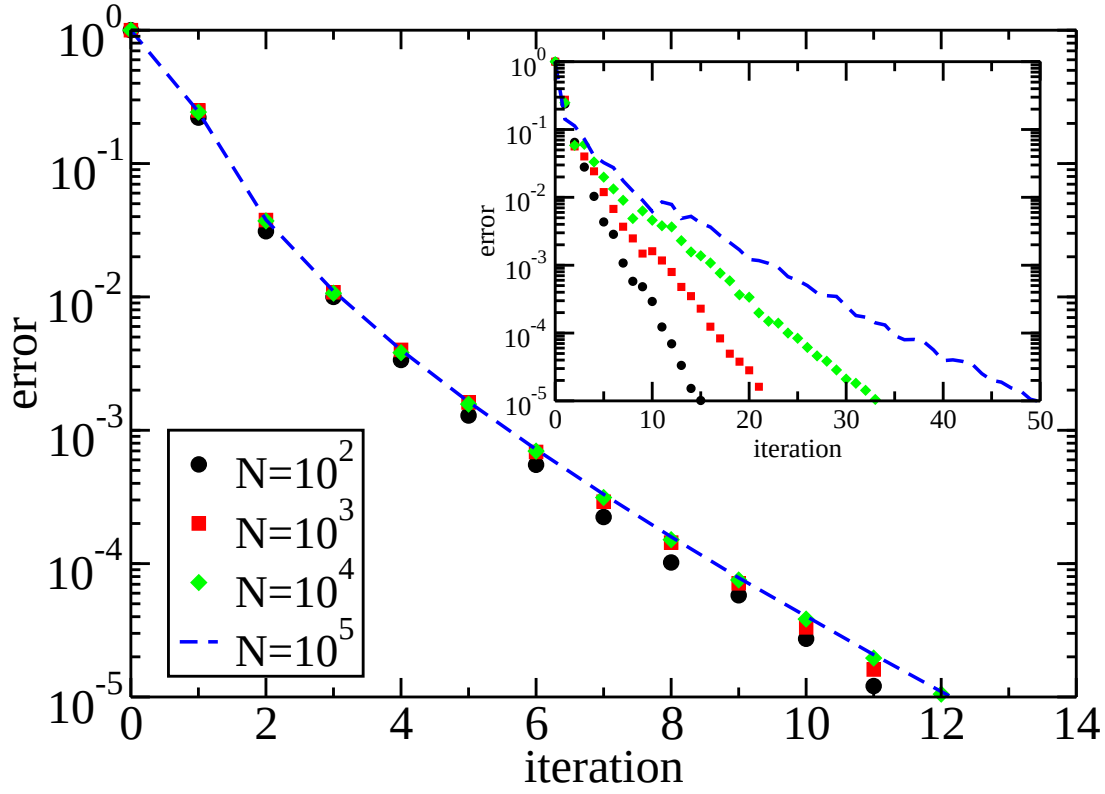

FIG. 1. Error versus iteration during the generation of the noise with the Lanczos algorithm for an equilibrium suspension of particles sedimented over the wall, for different number of particles N, keeping fixed the area fraction $\phi = 0.25$ and gravitational height (characteristic height over the wall) $h_g \approx 1.6a$. Similar results are obtained for a broad range of physically relevant gravitational heights. The inset shows the convergence of the Lanczos method for the same configurations when the screening of the hydrodynamic interactions by the wall is not included, i.e., the particle-particle hydrodynamic interactions decay as inverse of the distance.

C. Brownian noise

A key step in integrating the BD equation (1) using the scheme (3) or (4) is generating the noise term $\sqrt{2k_BT\Delta t}\boldsymbol{M}^{1/2}\boldsymbol{W}$. We compute the random term $\boldsymbol{M}^{1/2}\boldsymbol{W}$ with the Krylov method proposed by Ando et al. [27] (see also Section 3 in Ref. [39]). In short, we use the Lanczos algorithm with m iterations to compute the Krylov subspace $K_m(\boldsymbol{M}, \boldsymbol{W}) =$

span$\{\boldsymbol{W}, \boldsymbol{MW}, \ldots, (\boldsymbol{M})^{m-1}\boldsymbol{W}\}$ and to approximate the random noise, $\boldsymbol{g}_m \approx \boldsymbol{M}^{1/2}\boldsymbol{W}$, in that subspace. As in Ando el al. [27] we estimate the relative error ϵ_m at the mth iteration by the relative difference with the noise generated in the previous iteration, $\epsilon_m = \|\boldsymbol{g}_m - \boldsymbol{g}_{m-1}\|_2/\|\boldsymbol{g}_{m-1}\|_2$. The computational cost of this method is $\mathcal{O}(m^4 + m\mathrm{MV})$ where MV denotes the cost of computing one matrix vector product.

Figure 1 shows the Lanczos algorithm's convergence for suspensions with different number of particles sedimented over the wall. In general, iterative methods do not scale well for dense suspensions in three dimensions due to the slow $1/r$ decay of the Oseen/RPY tensor. The condition number of the mobility matrix increases with the system size which in turn increases the number of iterations to generate the noise. For particles in a half space, however, the situation is much better if the particles are confined in a thin layer next the wall. The wall screens the hydrodynamic interactions between particles, which decay like $1/r^3$ when $r \gg h$ [50], where h is the particles' height. We find that if particles are closer to the wall than they are to remote particles, the condition number is essentially independent of the number of particles, and in practice the Krylov method converges in a constant number of iterations. The results confirm that the convergence of the Krylov method is essentially independent of the number of particles and that less than a dozen iterations are required to reach a relative error tolerance $\sim 10^{-5}$ [64]. We note that as the particles start to overlap with the wall the condition number of the mobility matrix increases, however, the number of iteration is not affected for typical configurations (not shown).

We have tried to improve convergence of the Lanczos method by preconditioning [40]. A simple block diagonal preconditioner, which neglects the hydrodynamic interactions between distinct particles but does include the hydrodynamic interactions of each particle with the wall [14], gives only a very small improvement in the number of iterations. A preconditioner based on a incomplete Cholesky factorization of a truncated mobility matrix helps convergence greatly but also significantly increases the memory requirements and the complexity of the code, and also increases the cost per iteration. Therefore we do not use preconditioning [40] in this work.

To evaluate the screening effect of the wall on the Lanczos algorithm we compute the Brownian noise for the same particles configurations but neglecting the hydrodynamic interactions with the wall. The inset in Fig. 1 shows that the convergence worsens with increasing number of particles. For bulk suspensions either a preconditioned Krylov method [40]

or a direct (non-iterative) method [33] is needed to handle the ill-conditioning due to the long-ranged hydrodynamic interactions.

III. ACTIVE SUSPENSIONS: BROWNIAN ROLLERS

In this section, we perform Brownian Dynamics simulations of the fingering instability which was discovered in [7]. In that work, it was shown that suspensions of rollers (spherical particles) rotating parallel to a floor form narrow shock-like fronts which destabilize in the direction transverse to their motion. This transverse instability results in the formation of fingers with dense fingertips that propagate very fast compared to a single roller. Deterministic simulations showed that the wavelength of the fastest growing mode is set by the particles' height above the wall, which experiments suggest corresponds to the gravitational height. Here we assess how thermal noise affects the characteristic wavelength of the instability.

The experimental system consists of spherical colloidal particles of radius $a = 0.656\,\mu$m in which a small cube of hematite is embedded [52]. The hematite is a canted anti-ferromagnet and thus provide the rollers with a small permanent magnetic moment $|\mathbf{m}| = 5 \cdot 10^{-16}$ A·m^2. The particles are suspended in water ($\eta = 1$ mPa·s) at room temperature ($T = 300K$) at an average height from the wall given by the gravitational height $h_g = a + k_B T/mg$, which is set by the competition between gravity and Brownian motion. Here g denotes gravity and m the excess mass of the particles over the expelled fluid. The particles are rotated with an oscillating magnetic field $\mathbf{B} = B\left[\cos(\omega t)\hat{\mathbf{x}} + \sin(\omega t)\hat{\mathbf{z}}\right]$ with frequency $f = \omega/2\pi$ about the $\hat{\mathbf{y}}$ axis. If the field is strong enough and the frequency low enough to overcome the viscous torque exerted by the surrounding fluid, the particles rotate synchronously with $\mathbf{B}$ at a rate ω. In our previous deterministic simulations of the fingering instability [7], we kept the particle angular velocity fixed at ω, and computed the torque required to maintain that specified rotation. However, qualitatively identical behavior is observed if the particles are driven by a constant torque instead, which can also be realized experimentally and is somewhat cheaper to simulate. Therefore, here we exert a constant identical torque on every particle $\boldsymbol{T} = 8\pi\eta a^3\omega\hat{\mathbf{y}}$, where the driving frequency is in the experimental range, $\omega = 10\text{Hz} = 62.8\text{rad}/s$.

Due to the rotation a single particle will translate (roll) above the wall in the direction

perpendicular to the rotation. Additionally, the rotation creates a strong flow that can advect nearby particles. We can model these active flow effects by including in the right hand side of (1) the deterministic term $\boldsymbol{M}_C\boldsymbol{T}$ where $\boldsymbol{M}_C$ is the RPY translation-rotation mobility in the presence of a wall. For non-overlapping particles the equivalent of (5) gives the differential form of the RP translation-rotation mobility,

$$(\boldsymbol{M}_C)_{ij} = \boldsymbol{\mathcal{R}}_{\boldsymbol{\mathcal{C}}}\left(\boldsymbol{q}_i, \boldsymbol{q}_j\right) = \left(\boldsymbol{I} + \frac{a^2}{6}\boldsymbol{\nabla}_x^2\right)\left(\frac{1}{2}\boldsymbol{\nabla}_y\times\right)\boldsymbol{G}(\boldsymbol{x},\boldsymbol{y})\Big|_{\boldsymbol{x}=\boldsymbol{q}_i}^{\boldsymbol{y}=\boldsymbol{q}_j}, \tag{7}$$

and for overlapping particles one can use a suitable generalization of (6), see Eq. (3.16) in [44]. The final form of $\boldsymbol{\mathcal{R}}_{\boldsymbol{\mathcal{C}}}$ can be computed explicitly by adding the wall-corrections given in Eqs. (B2) and (C3) in [9] to the corresponding expression for an unbounded domain given in Eq. (3.16) in [44]. In the temporal integrators we treat the forcing term $\boldsymbol{M}_C\boldsymbol{T}$ like the deterministic force $\boldsymbol{MF}$.

We include a soft pairwise steric interaction $U(r)$ between the particles and between the particles and the wall to avoid severely limiting the time step size,

$$U(r) = \begin{cases} U_0 + U_0\frac{d-r}{b} & \text{if } r < d, \\ U_0\exp\left(-\frac{r-d}{b}\right) & \text{if } r \geq d. \end{cases} \tag{8}$$

For particle-particle interactions, $d = 2a$ and r is the distance between the centers of the particles, while for particle-wall interactions, $d = a$ and r is the distance of the center of the particle to the wall. The energy scale U_0 and interaction range b are parameters that control the strength and decay (range) of the potential. Even though the potential $U(r)$ does not strictly prevent a particle from crossing the wall, we can make the probability of such events arbitrarily small by setting the energy of a particle about to cross the wall to be very large compared with the thermal energy; in this paper we use $(1 + a/b)U_0 = 44k_BT$ and we never observe a particle escaping the physical domain in practice. The potential $U(r)$ introduces a characteristic steric time scale

$$\tau_U = \frac{6\pi\eta a^2 b}{U_0}. \tag{9}$$

We choose the values $U_0 = 4k_BT$ and $b = 0.1a$ to have a small number of overlaps but keeping τ_U no more than about an order of magnitude smaller than the other characteristic times in the system, the diffusive time $\tau_D = 3\pi\eta a^3/(k_BT)$ and the sedimentation time $\tau_g = 6\pi\eta a^2/(mg)$.

	$h = 1.5a$	$h = 3.5a$	$h = 6.1a$
Deterministic	9.4 s	17.3 s	32.6 s
Stochastic	11.8 s	26.9 s	42.9 s

TABLE I. Characteristic time $t^\star$ as defined in (10).

Each simulation contains $N = 2^{15} = 32,768$ particles which are initialized by sampling the equilibrium Gibbs-Boltzmann distribution of a two-periodic suspension with a periodic cell in the $x-y$ directions of extent $60a \times 4915a$ using a Monte Carlo method. The only parameter which is varied between the simulations is the gravitational height, $h_g = (1.5,\, 3.5,\, 6.1)a$, by changing the excess mass of the rollers, $m = (1,\, 0.2,\, 0.1) \times 1.27 \cdot 10^{-15}$ kg. The total simulation time is $40-160$ s depending on h_g, ensuring that the instability is well-developed for all gravitational heights. The tolerance of the Lanczos algorithm is $\epsilon_m = 10^{-3}$. The time step size is set to $\Delta t = 0.5\tau_U = 0.016$s to ensure that the correct Gibbs-Boltzmann equilibrium distribution is obtained for passive suspensions, see Appendix B, and to ensure that the active motion does not introduce significant overlaps; we have confirmed that essentially identical results are obtained by using $\Delta t = 0.008$s (not shown here). All the results below were averaged over four realizations for each case.

From the particle positions at a given time t we can compute the distribution $P(h)$ of particle heights h above the wall and the empirical number density $n(x, y; t)$ projected onto the $x-y$ plane. From $n(x, y; t)$ we compute two quantities of interest. The first quantity is the distribution of particle positions along the direction perpendicular to the unstable front, $\rho(x; t) = \int_y n(x, y; t)dy$. The second quantity is the Fourier transform of $n(x, y, t)$ at $k_x = 0$, i.e., the Fourier transform $\hat{n}(k_y = 2\pi/\lambda, t)$ of the number density along the direction of the front. In this second case we only use particles in the front, specifically, we only include the 70% of the particles with the largest x-coordinates. This ensures that the Fourier modes are not affected by the particles left behind the shock front. We have confirmed that essentially the same results are obtained when include between 50% and 90% of the particles. In order to compare the stochastic and deterministic simulations for various h, we define a characteristic time $t^\star$ as the time where $\hat{n}(k_y, t)$ reaches its maximum power,

$$t^\star = \underset{t}{\operatorname{argmax}} \int_{k_{\min}}^{k_{\max}} |\hat{n}(k_y, t)|^2 dk_y, \tag{10}$$

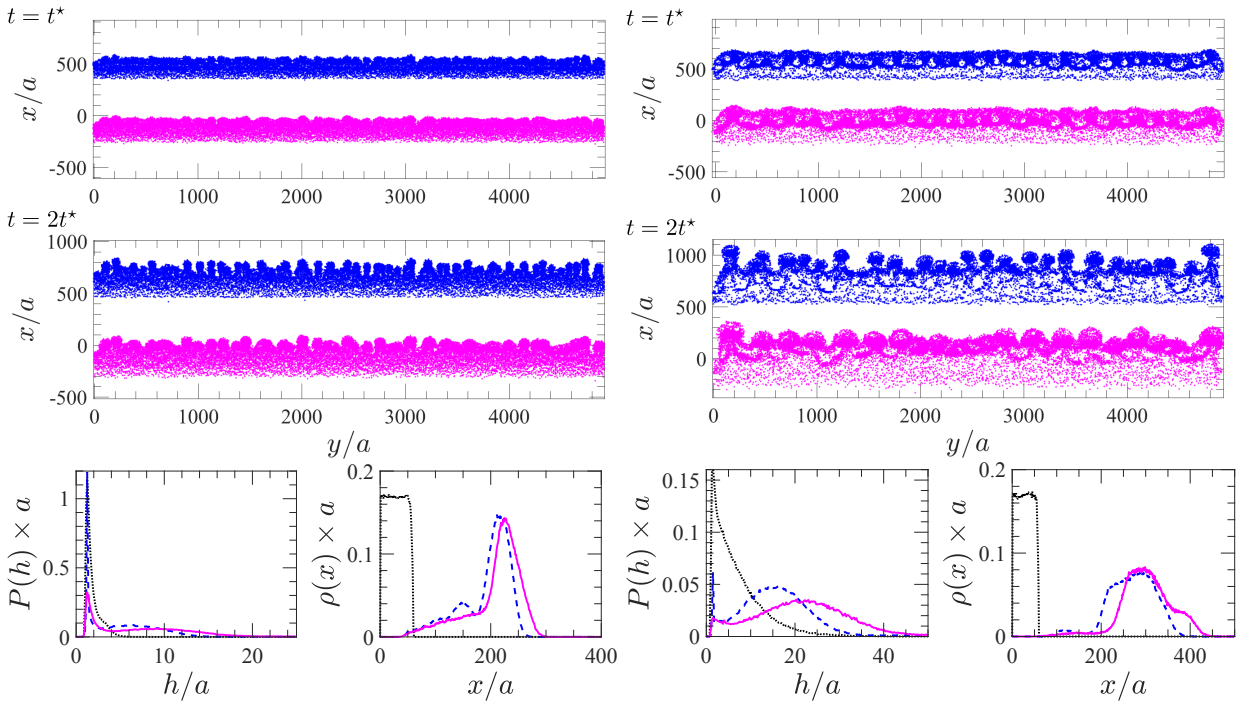

FIG. 2. Comparison between deterministic (blue) and stochastic (magenta) simulations at multiples of the characteristic time $t = t^\star$ given in Table I for two gravitational heights, $h_g = 1.5a$ (left half) and $h_g = 6.1a$ (right half). Top and middle subpanels: particle positions projected onto the $x - y$ plane (as would be observed in experiments) for a single realization, at $t = t^\star$ (top), when the instability begins to develop, and $t = 2t^\star$ (middle), when fingers have formed. The deterministic and stochastic results are staggered in the vertical direction for clarity. Bottom left subpanel: height distribution $P(h)$ at $t = t^\star$ averaged over four realizations. Bottom right subpanel: particle distribution $\rho(x)$ at $t = t^\star$ averaged over four realizations. In all bottom panels, the black dotted line show the initial distributions at $t = 0$ s.

where we choose $k_{\min} = 2.0 \cdot 10^{-3}$ μm^{-1} and $k_{\max} = 0.26$ μm^{-1}. Table I compares $t^\star$ between the deterministic and stochastic case. As shown by the value of $t^\star$, the dynamics in the Brownian system is slower than the deterministic one by about a factor of 1.4 for all three values of h_g. This difference in the time evolution is expected since the Brownian rollers spend more time farther away from the floor and thus translate slower.

Figure 2 compares the distributions of particle positions between the stochastic and deterministic simulations at $t = t^\star$ for two gravitational heights, $h_g = 1.5a$ and $h_g = 6.1a$; animated versions of these figures are available in the Supplementary Material. A visual

inspection reveals that the apparent wavelength of the instability is increased when thermal fluctuations are included in the system. In Fig. 3 we quantify this effect by comparing $|\hat{n}(k_y, t^\star)|^2$. At low wavenumbers the amplitude of the spectra is set by the active flow and is unaffected by the Brownian motion. At high wavenumbers the Brownian motion damps the amplitude of the spectra dramatically and this results in an effective shift of the spectra toward smaller wavenumbers, i.e. larger instability wavelengths, when thermal fluctuations are included. Diffusion also smears out the front, and the particle distribution $\rho(x)$ is smoother for the stochastic case at $t = t^\star$, see figure 2. Likewise, Brownian motion changes the particle distribution in the direction normal to the wall. Specifically, the peaks in $P(h)$, created by the active flows, are shifted toward larger heights and the peak close to the wall is less pronounced for the stochastic simulations. The discrepancy with the exponentially-decaying Gibbs-Boltzmann distribution (see $P(h)$ curves at $t = 0$ in Fig. 2) is due to active motion: the flow field generated in front of a roller close to a wall lifts the neighboring particles upwards (see Fig. 1c in [7]). It is also interesting to note that, in both cases, $P(h)$ is bi-modal when $h_g = 1.5a$ and tri-modal when $h_g = 6.1a$. This can be better appreciated in Figure 3 where the peaks of $P(h)$ are compared for all three gravitational heights. The existence of the third peak for $h_g = 6.1a$ is interesting in itself and requires more investigations to be fully explained. We suspect that enough rollers are located at the second peak to lift other particles even higher.

These results support our previous observations that the gravitational height, which sets the initial height of the particles above the floor, plays a predominant role in the selection of the fastest growing mode [7]. Here, as in the experiments, the gravitational height is controlled by the Brownian diffusion in the direction perpendicular to the wall. Note that our initial conditions are similar, but not identical, to the experiments, where the particles reach an approximately quasi-steady equilibrium configuration in a narrow strip. Our studies also show that Brownian motion doesn't just control the initial condition but also quantitatively, though not qualitatively, affects the subsequent evolution of the fingering instability. We can estimate a Péclet number as $\mathrm{Pe} = v(h_g - a)/D$, where $D = k_B T/(6\pi\eta a)$ is a typical diffusion coefficient and the characteristic speed is estimated as $v = x_f(t^\star)/t^\star$ where the front position $x_f(t)$ is the location of the maximum in $\rho(x;t)$. This leads to values in the range $\mathrm{Pe} \sim 12 - 45$ for our parameters, which indicates that the motion is dominated by the active flows. In this specific example, however, the thermal fluctuations are still important because

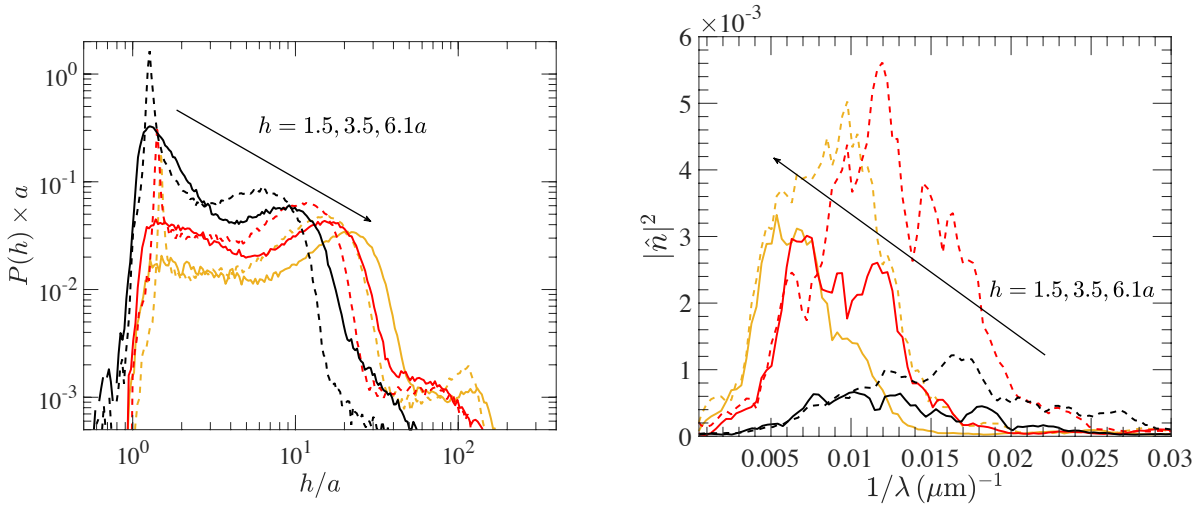

FIG. 3. Comparison between deterministic (dashed lines) and stochastic (solid lines) simulations at the characteristic time $t = t^\star$ given in Table I. Results are shown for three gravitational heights, $h = 1.5a$ (black), $3.5a$ (red) and $6.1a$ (orange), and averaged over four realizations. Left: log-log plot of the height distribution $P(h)$. Right: Fourier spectrum $|\hat{n}(2\pi/\lambda, t^\star)|^2$ of the fluctuations along the front.

they strongly affect the height distribution and the height determines both the time scale and the wavelength of the fingering instability. It is also worthwhile mentioning that our stochastic simulations are in quantitative agreement with the experimental measurements. The predominant wavelength in our stochastic simulations at $t = t^\star$ is $\lambda_{\text{num}} = 98\ \mu$m for $h_g = 1.5a$ and $\lambda_{\text{num}} = 140\ \mu$m for $h_g = 3.5a$, which is in good agreement with the fastest growing mode measured in the experiments for similar gravitational heights: $\lambda_{\text{exp}} \approx 95\ \mu$m and $\lambda_{\text{exp}} \approx 160\ \mu$m respectively [7].

IV. CONCLUSIONS

In this paper we presented tools to perform efficient Brownian dynamics simulations in a half-space. We proposed a stochastic Adams-Bashforth method, in which we discretize the deterministic terms using a linear two-step method, and include the non-trivial stochastic drift using a random finite difference [30]. In Appendix A we present an approach for retaining the positive definiteness of the mobility matrix even if the system reaches an unphysical configuration. We demonstrated that we can use the Lanczos algorithm [27, 39] to generate

the Brownian noise in a small number of iterations independent of the number of particles. Our simulations in Sec. III illustrate the capacity of our numerical methods to effectively simulate suspensions of tens to hundreds of thousands of active Brownian particles confined near a no-slip boundary over realistic conditions and timescales. We showed that Brownian motion affects quantitatively, but not qualitatively, the development of a fingering instability observed in active roller suspensions [7]. Our PyCUDA codes are publicly available at `https://github.com/stochasticHydroTools/RigidMultiblobsWall`.

Our simple GPU implementation of the procedure to multiply a vector of forces by the mobility matrix scales quadratically with the number of particles. If one wishes to study very large systems with many hundreds of thousands of particles, one ought to use a linear scaling method such as the FMM. It is therefore an important direction for future work to generalize the point Stokeslet FMM developed in Ref. [49] to the RPY tensor. Note that in FMM methods the near-field interactions are computed directly so no special effort is needed to handle overlapping particles. However, as we discussed in the body of this paper, handling overlaps with the wall requires switching from the differential form of the RPY tensor (5), which is amenable to standard multipole techniques [39], to the integral form (6), which is harder to handle using stnadard multipole expansions.

The method described here only requires a procedure to apply the mobility matrix to a vector. As such, it can in principle be generalized to other cases where explicit formulas for the mobility matrix are available. For example, recently the RP tensor has been computed for particles confined in a spherical cavity [53]. However, the key difficulty is that the Lanczos iterative method for computing the Brownian increments is not going to converge in a constant number of iterations, independent of the number of particles, unless that hydrodynamic interactions are strongly screened. Somewhat suprisingly, for particles confined to a slit channel with no-slip walls [54], the hydrodynamic interactions decay *slower* than they do for particles near a single no-slip boundary; it is known that the decay is $1/r^2$ instead of the $1/r^3$ as in the case studied here [50]. It is an interesting question for future study to explore how well the Lanczos iterative method converges for suspensions in a thin slit channel, a situation of great practical interest. For bulk three-dimensional suspensions it is known that the conditioning number of the RPY mobility matrix increases with the number of particles. For periodic boundary conditions, a new linear scaling method to compute the Brownian increments has recently been proposed. In this Positively Split Ewald method [33]

one employs an Ewald method to split the hydrodynamic interactions into near- and far-field interactions. The near-field interactions are then handled using the Lanczos method, which converges in a small number of iterations, and the far-field interactions are treated using fluctuating hydrodynamics.

In this work we only considered the RPY tensor, which captures the far-field hydrodynamic interactions but does not accurately model near-field hydrodynamics. There are several techniques that can go beyond the RPY tensor. The first approach, which is useful for spherical particles, is to use multipole expansions of higher order. This has been done systematically via a Galerkin truncation in recent work by Singh and Adhikari [11]; when truncated at the level of stresslets this approach is closely-related to the widely-used method of Stokesian dynamics [9]. The Galerkin approach ensures an SPD mobility matrix so Brownian motion can be added straightforwardly, however, the key difficulty lies in efficient implementation for systems of many particles. Another approach is to use boundary integral methods [55, 56], which explicitly discretize the boundary and are thus more general. These methods do not ensure an SPD matrix, and are also still too expensive to use for suspensions of thousands of particles. Another issue is that both multipole expansion and boundary integral methods break down when particles (nearly) overlap each other or the wall. This makes handling Brownian motion difficult. A third approach is to represent colloidal particles as rigid multiblobs constructed by rigidly connecting "blobs" that interact hydrodynamically via the RPY tensor [14, 57]. This method requires the same building blocks as we used here, and thermal fluctuations can be added in a natural way using the Lanczos method applied to the blob-blob RPY mobility. In future work we will explore such rigid multilbob methods for Brownian dynamics near a no-slip boundary.

V. SUPPLEMENTARY MATERIAL

See supplementary material for animated versions of figure 2 for gravitational heights $h_g = 1.5a$, $3.5a$, and $6.1a$.

VI. ACKNOWLEDGMENT

We are grateful to Paul Chaikin and Michelle Driscoll for numerous discussions regarding the fingering instability in active roller suspensions, and to Edmond Chow for discussions of the Lanczos method. This work was supported in part by the National Science Foundation under award DMS-1418706, and by the U.S. Department of Energy Office of Science, Office of Advanced Scientific Computing Research, Applied Mathematics program under Award Number DE-SC0008271. B. Delmotte was supported partially by the Materials Research Science and Engineering Center (MRSEC) program of the National Science Foundation under Award Number DMR-1420073. We thank the NVIDIA Academic Partnership program for providing GPU hardware for performing the simulations reported here.

Appendix A: SPD mobility matrix

In this Appendix we propose a method to regularize the mobility matrix to allow for particle-wall overlaps. Since overlap with the wall is unphysical there is no unique choice of how to define the pairwise mobility, and existing literature on the RPY tensor in the presence of a wall does not address this question [9, 44]. There are two physical requirements, however, that any proposal must satisfy. The first is that a particle whose center touches the wall must stop moving regardless of what forces are applied to it or to other particles. This ensures that a particle cannot leave the domain and cross through the wall even in the presence of noise, because the Brownian displacement of a particle that is about to leave the wall also vanishes if the particle's mobility vanishes. More precisely, we want the self-mobility $\boldsymbol{M}_{ii}$ and the cross-mobilities $\boldsymbol{M}_{ij}$ go to zero smoothly as the overlap between particle i and the wall increases. The second requirement is that the mobility matrix must remain SPD for all particle configurations.

Yeo and Maxey proposed a strategy to define the pairwise mobility for particles overlapping a boundary in the context of the Force Coupling Method (FCM) [58], and this was subsequently generalized to more general types of boundary conditions in the context of the Immersed Boundary method [14, 59]. The idea is to replace the integrals over the particle surface in Eq. (6) by volume integrals on the physical domain (half-space above the wall) Ω and to subtract the effect of an image particle located beyond the wall, leading to the

general definition of the Rotne-Prager-Yamakawa (RPY) tensor in the presence of a wall,

$$\begin{aligned}\boldsymbol{\mathcal{R}}\left(\boldsymbol{q}_i,\boldsymbol{q}_j\right) = \frac{1}{(4\pi a^2)^2}\int_\Omega d\boldsymbol{x}\int_\Omega d\boldsymbol{y}\;\boldsymbol{G}(\boldsymbol{x},\boldsymbol{y}) \\ \cdot\left(\delta(|\boldsymbol{x}-\boldsymbol{q}_i|-a)-\delta(|\boldsymbol{x}-\boldsymbol{q}_i^{im}|-a)\right) \\ \cdot\left(\delta(|\boldsymbol{y}-\boldsymbol{q}_j|-a)-\delta(|\boldsymbol{y}-\boldsymbol{q}_j^{im}|-a)\right)\end{aligned} \tag{A1}$$

where $\delta(x)$ is the Dirac delta function and the image particle is located at $\boldsymbol{q}_i^{im} = \boldsymbol{q}_i - 2\hat{\boldsymbol{e}}_z(\hat{\boldsymbol{e}}_z\cdot\boldsymbol{q}_i)$, where we take the z axis to be perpendicular to the wall and directed into the domain. Unfortunately, the expression (A1) involves complicated integrals that cannot, to our knowledge, be computed analytically.

Instead, as an alternative to (A1) in this paper we use an *ad hoc* approximation to define a mobility that satisfies the physical requirements yet is trivial to compute. We take

$$\boldsymbol{M} = \boldsymbol{B}\widetilde{\boldsymbol{M}}\boldsymbol{B}, \tag{A2}$$

where $\boldsymbol{B}$ is a diagonal matrix with diagonal blocks

$$\boldsymbol{B}_{ii} = H_0\left(z_i/a\right)\boldsymbol{I}, \tag{A3}$$

where the smoothed Heaviside function H_0 is

$$H_0(x) = \begin{cases} 1 & \text{if } x > 1, \\ x & \text{if } 0 \le x \le 1 \\ 0 & \text{if } x < 0. \end{cases} \tag{A4}$$

The regularized mobility matrix $\widetilde{\boldsymbol{M}}$ is the mobility given (6) but always evaluated for configurations in which neither particle overlaps the wall,

$$\widetilde{\boldsymbol{M}}_{ij} = \boldsymbol{\mathcal{R}}\left((x_i,y_i,\max(z_i,a)),\,(x_j,y_j,\max(z_j,a))\right). \tag{A5}$$

As desired, the mobility matrix defined by (A2) and (A1) is SPD for all configurations and its sub-blocks $\boldsymbol{M}_{ij}$ smoothly go to zero as either particle i or j overlaps the wall. We note that the *ad hoc* approximations like Eq. (A2) may be useful for other Langevin equations where the system can reach an unphysical state for which the mobility is either undefined or not SPD, or both. This approach is much simpler and more efficient than trying to strictly prevent unphysical configurations, as in Metropolis schemes [60]. It is important to ensure, however, that the Heaviside regularization is only applied infrequently, and therefore does not affect the results significantly. We ensure this here by including a repulsive potential (8) with the wall.

Appendix B: Temporal accuracy

In this Appendix, we validate and test the accuracy of our numerical schemes on equilibrium systems by comparing the equilibrium distribution sampled by the BD with the desired Gibbs-Boltzmann distribution, which we can sample "exactly" using a standard Markov Chain Monte Carlo (MCMC) method [61]. Specifically, we examine here the distribution $P(h)$ of particle heights h above the wall, as well as the distribution of pairwise distances given by the pair correlation function $g(r)$. Because the system is quasi-two-dimensional, we define the radial distribution $g(r)$ using the three-dimensional distance $r = (x^2+y^2+z^2)^{1/2}$, but normalize the probability density function as if the suspension were two-dimensional. This ensures that $g(r)$ goes to unity for $r \gg a$ and that $g(r < 2a) = 0$ for a hard-sphere suspension. In the equilibrium simulations we use pseudo-periodic boundary conditions (PPBC) in the two directions parallel to the wall. We compute the forces $\boldsymbol{F}$ using the minimum image convention between particles as with standard Periodic Boundary Conditions. To account for the longer range of the hydrodynamic interactions we consider hydrodynamic interactions between particles in the unit cell and in the first eight neighbor cells, similarly to what is done in [62]. We can reduce the truncation error in the hydrodynamic interactions by including the effect of particles in further neighbor cells (see Ref. [62] for some fast approximations); because the screened hydrodynamic interactions decay fast with the distance this sum is absolutely convergent. A more sophisticated approach will be to use a variation of the Ewald's summation method [63]. However, for validating the scheme we do not need to refine our approximation because in the Stokes regime the equilibrium distribution is *n*ot affected by the hydrodynamic interactions. The only necessary requirement is to use the same mobility in the stochastic and deterministic parts of the schemes to obey the fluctuation dissipation balance. In the numerical experiments of section III we did not use PPBC since the experiments [7] are performed in a finite sample and not in a bulk suspension.

In Fig. 4 we show $P(h)$ and the error in $g(r)$ (recall that the scale for $g(r \gg a) \approx 1$) for BD performed using the EM (3) and AB (4) schemes, for several time step sizes Δt and the parameters given in Section III. The tolerance of the Lanczos algorithm is set to $\epsilon_m = 10^{-4}$. The fact that the correct equilibrium GB distribution is obtained for small Δt indicates that fluctuation-dissipation is preserved by our temporal integration schemes because the stochastic drift term is correctly captured by the RFD. For large time step sizes

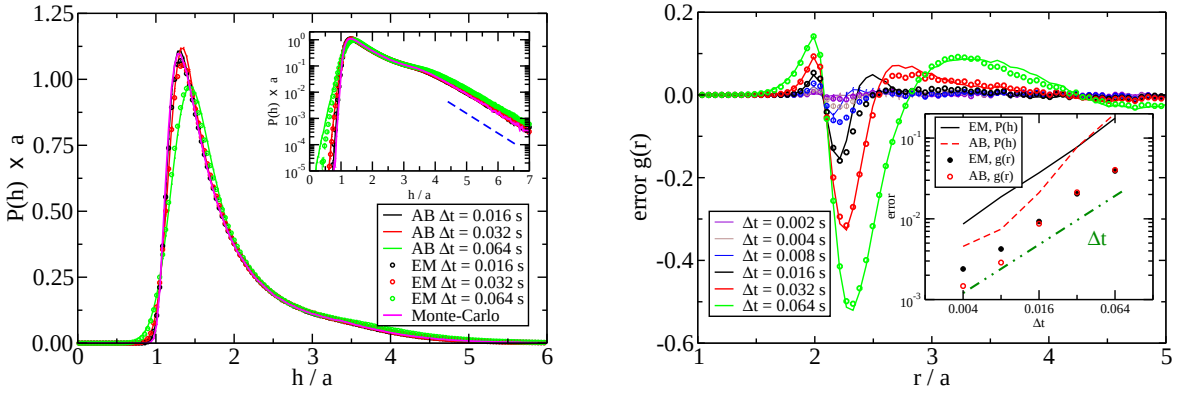

FIG. 4. Stochastic accuracy of the Euler-Maruyama and Adams-Bashforth schemes for several time step sizes, for a pseudo-periodic passive suspension of $N = 1000$ particles, with area fraction $\phi = 0.25$, $U_0 = 4k_BT$, $b = 0.1a$ and $h_g = 1.58a$. The left panel compares the histogram of particle heights $P(h)$ to the "exact" distribution sampled by a Monte-Carlo method. The inset shows the exponential decay $\sim \exp(-mgh/k_BT)$ (dashed line) due to the gravity field, as well as the increased probability of particle-wall overlaps when Δt is larger than the steric time $\tau_U = 0.032\,s$. The right panel shows the error in the radial distribution function $g(r)$ with respect to the exact result (computed with a Monte-Carlo method) for the EM scheme (dots) and AB scheme (lines). The inset shows the L_2 norm of the error in $P(h)$ and $g(r)$ versus the time step size, demonstrating the first-order weak accuracy of both methods. We can see that for sufficiently small time step sizes AB is more accurate than the EM scheme.

compared with the steric characteristic time, such as for example $\Delta t = 2\tau_U = 0.064\,s$, the results show a large deviation with respect to the Monte Carlo results. We can see also that the probability of overlap between particles and the wall becomes non-negligible. However, when the time step size is not too large compared with the steric characteristic time, for example $\Delta t \leq 0.5\tau_U = 0.016\,s$, the agreement between MCMC and BD simulations is quite good. The average/overall error in the histograms as a function of Δt is shown in the inset in the right panel in Fig. 4. We see that the AB scheme (4) is more accurate than the EM scheme (3) except for the time step sizes that do not resolve the relevant time scales, in

which case both schemes are similar.

---

[1] Jesús Santana-Solano, Angeles Ramírez-Saito, and José Luis Arauz-Lara. Short-time dynamics in quasi-two-dimensional colloidal suspensions. *Phys. Rev. Lett.*, 95:198301, Oct 2005.

[2] Ayan Chakrabarty, Andrew Konya, Feng Wang, Jonathan V Selinger, Kai Sun, and Qi-Huo Wei. Brownian motion of boomerang colloidal particles. *Physical review letters*, 111(16):160603, 2013.

[3] KH Lan, N Ostrowsky, and D Sornette. Brownian dynamics close to a wall studied by photon correlation spectroscopy from an evanescent wave. *Physical review letters*, 57(1):17, 1986.

[4] Daisuke Takagi, Jeremie Palacci, Adam B. Braunschweig, Michael J. Shelley, and Jun Zhang. Hydrodynamic capture of microswimmers into sphere-bound orbits. *Soft Matter*, 10:1784, 2014.

[5] Megan Davies Wykes, Jeremie Palacci, Takuji Adachi, Leif Ristroph, Yanpeng Liu, Xiao Zhong, Jun Zhang, Michael Ward, and Michael Shelley. Dynamic self-assembly of microscale rotors and swimmers. *Soft Matter*, 12:4584, 2016.

[6] Jeremie Palacci, Stefano Sacanna, Asher Preska Steinberg, David J Pine, and Paul M Chaikin. Living crystals of light-activated colloidal surfers. *Science*, 339(6122):936–940, 2013.

[7] Michelle Driscoll, Blaise Delmotte, Mena Youssef, Stefano Sacanna, Aleksandar Donev, and Paul Chaikin. Unstable fronts and motile structures formed by microrollers. *Nature Physics*, 2016. Published online (doi:10.1038/nphys3970), preprint ArXiv:1609.08673.

[8] Allison P. Berke, Linda Turner, Howard C. Berg, and Eric Lauga. Hydrodynamic attraction of swimming microorganisms by surfaces. *Phys. Rev. Lett.*, 101:038102, Jul 2008.

[9] James W. Swan and John F. Brady. Simulation of hydrodynamically interacting particles near a no-slip boundary. *Physics of Fluids*, 19(11):113306, 2007.

[10] V. N. Michailidou, G. Petekidis, J. W. Swan, and J. F. Brady. Dynamics of concentrated hard-sphere colloids near a wall. *Phys. Rev. Lett.*, 102:068302, Feb 2009.

[11] Rajesh Singh and R. Adhikari. Universal hydrodynamic mechanisms for crystallization in active colloidal suspensions. *Phys. Rev. Lett.*, 117:228002, 2016.

[12] Saverio E Spagnolie and Eric Lauga. Hydrodynamics of self-propulsion near a boundary: predictions and accuracy of far-field approximations. *Journal of Fluid Mechanics*, 700:105–

147, 2012.

[13] Enkeleida Lushi, Vasily Kantsler, and Raymond E. Goldstein. Scattering of bi-flagellate microswimmers from surfaces. arXiv:1608.02551, 2016.

[14] F. Balboa Usabiaga, B. Kallemov, B. Delmotte, A. P. S. Bhalla, B. E. Griffith, and A. Donev. Hydrodynamics of suspensions of passive and active rigid particles: a rigid multiblob approach. *Communications in Applied Mathematics and Computational Science*, 11(2):217–296, 2016.

[15] Rajesh Singh, Somdeb Ghose, and R Adhikari. Many-body microhydrodynamics of colloidal particles with active boundary layers. *Journal of Statistical Mechanics: Theory and Experiment*, 2015(6):P06017, 2015.

[16] Alexander P. Petroff, Xiao-Lun Wu, and Albert Libchaber. Fast-moving bacteria self-organize into active two-dimensional crystals of rotating cells. *Phys. Rev. Lett.*, 114:158102, Apr 2015.

[17] Enkeleida Lushi and Petia M Vlahovska. Periodic and chaotic orbits of plane-confined microrotors in creeping flows. *Journal of Nonlinear Science*, 25(5):1111–1123, 2015.

[18] Kyongmin Yeo, Enkeleida Lushi, and Petia M Vlahovska. Collective dynamics in a binary mixture of hydrodynamically coupled microrotors. *Physical review letters*, 114(18):188301, 2015.

[19] Kenta Ishimoto and Eamonn A. Gaffney. A study of spermatozoan swimming stability near a surface. *Journal of Theoretical Biology*, 360:187 – 199, 2014.

[20] A. J. T. M. Mathijssen, D. O. Pushkin, and J. M. Yeomans. Tracer trajectories and displacement due to a micro-swimmer near a surface. *Journal of Fluid Mechanics*, 773:498–519, Jun 2015.

[21] Sambeeta Das, Astha Garg, Andrew I Campbell, Jonathan Howse, Ayusman Sen, Darrell Velegol, Ramin Golestanian, and Stephen J Ebbens. Boundaries can steer active janus spheres. *Nature communications*, 6, 2015.

[22] Pushkar P. Lele, James W. Swan, John F. Brady, Norman J. Wagner, and Eric M. Furst. Colloidal diffusion and hydrodynamic screening near boundaries. *Soft Matter*, 7:6844–6852, 2011.

[23] John F. Brady and George Bossis. Stokesian dynamics. *Annual Review of Fluid Mechanics*, 20:111, 1988.

[24] Adolfo J Banchio and John F Brady. Accelerated stokesian dynamics: Brownian motion. *The Journal of chemical physics*, 118:10323, 2003.

[25] Marshall Fixman. Construction of langevin forces in the simulation of hydrodynamic interaction. *Macromolecules*, 19(4):1204–1207, 1986.

[26] Richard M. Jendrejack, Michael D. Graham, and Juan J. de Pablo. Hydrodynamic interactions in long chain polymers: Application of the chebyshev polynomial approximation in stochastic simulations. *Journal of Chemical Physics*, 113(7):2894, 2000.

[27] Tadashi Ando, Edmond Chow, Yousef Saad, and Jeffrey Skolnick. Krylov subspace methods for computing hydrodynamic interactions in brownian dynamics simulations. *The Journal of Chemical Physics*, 137(6):–, 2012.

[28] Juan P Hernández-Ortiz, Patrick T Underhill, and Michael D Graham. Dynamics of confined suspensions of swimming particles. *Journal of Physics: Condensed Matter*, 21(20):204107, 2009.

[29] Sandeep Chilukuri, Cynthia H Collins, and Patrick T Underhill. Impact of external flow on the dynamics of swimming microorganisms near surfaces. *Journal of Physics: Condensed Matter*, 26(11):115101, 2014.

[30] S. Delong, F. Balboa Usabiaga, R. Delgado-Buscalioni, B. E. Griffith, and A. Donev. Brownian Dynamics without Green's Functions. *J. Chem. Phys.*, 140(13):134110, 2014. Software available at `https://github.com/stochasticHydroTools/FIB`.

[31] J. P. Hernandez-Ortiz, J. J. de Pablo, and M. D. Graham. Fast Computation of Many-Particle Hydrodynamic and Electrostatic Interactions in a Confined Geometry. *Phys. Rev. Lett.*, 98(14):140602, 2007.

[32] Blaise Delmotte and Eric E Keaveny. Simulating brownian suspensions with fluctuating hydrodynamics. *The Journal of chemical physics*, 143(24):244109, 2015.

[33] A. M. Fiore, F. Balboa Usabiaga, A. Donev, and J. W. Swan. Rapid Sampling of Stochastic Displacements in Brownian Dynamics Simulations. To appear in J. Chem. Phys., Arxiv:1611.09322, 2016.

[34] M. Fixman. Simulation of polymer dynamics. I. General theory. *J. Chem. Phys.*, 69:1527, 1978.

[35] L. Durlofsky, J. F. Brady, and G. Bossis. Dynamic simulation of hydrodynamically interacting particles. *Journal of Fluid Mechanics*, 180:21, 1987.

[36] Kengo Ichiki. Improvement of the stokesian dynamics method for systems with a finite number of particles. *Journal of Fluid Mechanics*, 452:231–262, 2002. See `http://kichiki.github.`

com/libstokes/ for software.

[37] Eric E. Keaveny. Fluctuating force-coupling method for simulations of colloidal suspensions. *J. Comp. Phys.*, 269(0):61 – 79, 2014.

[38] S. Delong, F. Balboa Usabiaga, and A. Donev. Brownian dynamics of confined rigid bodies. *J. Chem. Phys.*, 143(14), 2015. Software available at `https://github.com/stochasticHydroTools/RotationalDiffusion`.

[39] Zhi Liang, Zydrunas Gimbutas, Leslie Greengard, Jingfang Huang, and Shidong Jiang. A fast multipole method for the rotne–prager–yamakawa tensor and its applications. *Journal of Computational Physics*, 234:133–139, 2013.

[40] Edmond Chow and Yousef Saad. Preconditioned krylov subspace methods for sampling multivariate gaussian distributions. *SIAM Journal on Scientific Computing*, 36(2):A588–A608, 2014.

[41] Renfeng Cao and Stephen B. Pope. Numerical integration of stochastic differential equations: weak second-order mid-point scheme for application in the composition pdf method. *Journal of Chemical Physics*, 185:194, 2002.

[42] A Abdulle, G Vilmart, and K Zygalakis. Weak second order explicit stabilized methods for stiff stochastic differential equations. *SIAM J. Sci. Comput.*, 35(4):A1792–A1814, 2013.

[43] S. Delong, B. E. Griffith, E. Vanden-Eijnden, and A. Donev. Temporal Integrators for Fluctuating Hydrodynamics. *Phys. Rev. E*, 87(3):033302, 2013.

[44] Eligiusz Wajnryb, Krzysztof A Mizerski, Pawel J Zuk, and Piotr Szymczak. Generalization of the rotne–prager–yamakawa mobility and shear disturbance tensors. *Journal of Fluid Mechanics*, 731:R3, 2013.

[45] J.R. Blake and A.T. Chwang. Fundamental singularities of viscous flow. *Journal of Engineering Mathematics*, 8(1):23–29, 1974.

[46] Jens Rotne and Stephen Prager. Variational treatment of hydrodynamic interaction in polymers. *The Journal of Chemical Physics*, 50:4831, 1969.

[47] Andreas Klöckner, Nicolas Pinto, Yunsup Lee, B. Catanzaro, Paul Ivanov, and Ahmed Fasih. PyCUDA and PyOpenCL: A Scripting-Based Approach to GPU Run-Time Code Generation. *Parallel Computing*, 38(3):157–174, 2012.

[48] Michael Kopp and Felix Höfling. Gpu-accelerated simulation of colloidal suspensions with direct hydrodynamic interactions. *The European Physical Journal Special Topics*, 210(1):101–

117, 2012.

[49] Z. Gimbutas, L. Greengard, and S. Veerapaneni. Simple and efficient representations for the fundamental solutions of Stokes flow in a half-space. *Journal of Fluid Mechanics*, 776:R1, 2015. Code available at `http://www.cims.nyu.edu/cmcl/fmm3dlib/fmm3dlib.html`.

[50] Haim Diamant. Hydrodynamic interaction in confined geometries. *Journal of the Physical Society of Japan*, 78(4):041002, 2009.

[64] The fact the mobility matrix is well-conditioned makes it also possible to use Fixman's midpoint scheme in practice instead of the RFD, since one can use the Lanczos method to efficiently compute $\boldsymbol{M}^{1/2}\boldsymbol{W}$ and $\boldsymbol{M}^{-1/2}\boldsymbol{W}$ together.

[52] Stefano Sacanna, Laura Rossi, and David J Pine. Magnetic click colloidal assembly. *Journal of the American Chemical Society*, 134(14):6112–6115, 2012.

[53] Christian Aponte-Rivera and Roseanna N. Zia. Simulation of hydrodynamically interacting particles confined by a spherical cavity. *Phys. Rev. Fluids*, 1:023301, 2016.

[54] James W Swan and John F Brady. Particle motion between parallel walls: Hydrodynamics and simulation. *Physics of Fluids*, 22:103301, 2010.

[55] Ludvig Af Klinteberg and Anna-Karin Tornberg. Fast ewald summation for stokesian particle suspensions. *International Journal for Numerical Methods in Fluids*, 76(10):669–698, 2014.

[56] Oana Marin, Katarina Gustavsson, and Anna-Karin Tornberg. A highly accurate boundary treatment for confined stokes flow. *Computers & Fluids*, 66:215–230, 2012.

[57] James W Swan and Gang Wang. Rapid calculation of hydrodynamic and transport properties in concentrated solutions of colloidal particles and macromolecules. *Physics of Fluids (1994-present)*, 28(1):011902, 2016.

[58] Kyongmin Yeo and Martin R Maxey. Dynamics of concentrated suspensions of non-colloidal particles in couette flow. *Journal of Fluid Mechanics*, 649(1):205–231, 2010.

[59] B. Kallemov, A. Pal Singh Bhalla, B. E. Griffith, and A. Donev. An immersed boundary method for rigid bodies. *Communications in Applied Mathematics and Computational Science*, 11(1):79–141, 2016. Software available at `https://github.com/stochasticHydroTools/RigidBodyIB`.

[60] N. Bou-Rabee, A. Donev, and E. Vanden-Eijnden. Metropolis Integration Schemes for Self-Adjoint Diffusions. *SIAM J. Multiscale Modeling and Simulation*, 12(2):781–831, 2014.

[61] M. P. Allen and D. J. Tildesley. *Computer Simulations of Liquids*. Oxford Science Publications,

1987.

[62] Natan Osterman and Andrej Vilfan. Finding the ciliary beating pattern with optimal efficiency. *Proceedings of the National Academy of Sciences*, 108(38):15727–15732, 2011.

[63] Hoang-Ngan Nguyen and Karin Leiderman. Computation of the singular and regularized image systems for doubly-periodic stokes flow in the presence of a wall. *Journal of Computational Physics*, 297:442–461, 2015.

[64] The fact the mobility matrix is well-conditioned makes it also possible to use Fixman's midpoint scheme in practice instead of the RFD, since one can use the Lanczos method to efficiently compute $\boldsymbol{M}^{1/2}\boldsymbol{W}$ and $\boldsymbol{M}^{-1/2}\boldsymbol{W}$ together.